Supporting Information

Coating and Stabilization of Liposomes by Clathrin-Inspired DNA Self-Assembly

Kevin N. Baumann[1], Luca Piantanida[2†], Javier García-Nafría[3‡‖], Diana Sobota[4], Kislon Voïtchovsky[2], Tuomas P. J. Knowles[1,4], Silvia Hernández-Ainsa[5,6,7*]*

[1]University of Cambridge, Department of Chemistry, Lensfield Road, CB2 1EW, Cambridge, United Kingdom

[2]University of Durham, Department of Physics, Durham DH1 3LE, United Kingdom

[3]MRC Laboratory of Molecular Biology, CB2 0QH, Cambridge, United Kingdom

[4]University of Cambridge, Cavendish Laboratory, CB3 0HE, Cambridge, United Kingdom

[5]Instituto de Nanociencia de Aragón, University of Zaragoza, 50018, Zaragoza, Spain

[6]Instituto de Ciencia de Materiales de Aragón, University of Zaragoza-CSIC, 50009, Zaragoza, Spain

[7]ARAID foundation, Government of Aragon, 50018, Zaragoza, Spain

Current addresses:

† Micron School of Materials Science & Engineering, Boise State University, Boise, ID 83725, USA

‡ Institute of Biocomputation and Physics of Complex Systems (BIFI), University of Zaragoza, BIFI-IQFR (CSIC), 50018, Zaragoza, Spain

‖ Laboratorio de Microscopías Avanzadas, University of Zaragoza, 50018, Zaragoza, Spain

List of contents

S1. Details on DNA sequences and assembly protocol

The tables Table S1 to Table S5 list the sequences used for the fabrication of the linker (Table S1), triskelion (Table S2), the non-hybridizing triskelion (Table S3), the removable triskelion (Table S4), and the displacement strand (Table S5). The oligonucleotide concentrations of the stocks were adjusted prior to folding, based on absorption measurements at 260 nm (Nanodrop 2000, Fisher Scientific).

Table S1. Oligonucleotide sequences of the linker strands. "CholTEG" indicates the position of the cholesterol-TEG modification

Oligo name	Sequence
L1	5'-TCTCTTTGGATAATCTTC CCTCTGCTGCCGCTCAAG-3'/CholTEG
L2	5'-TCTCTTTGGATAATCTTC CTTGAGCGGCAGCAGAGG-3'

Table S2. Oligonucleotide sequences of the three triskelion designs.

Oligo name	Sequence
T1-S1	5'-GAAGATTATCCAAAGAGA TCCGAGTTGTCTTGTACA **T** CCTGAAGATACATCAAGC-3'
T1-S2	5'-GAAGATTATCCAAAGAGA GGTAGGCTAGTATCTGTG **T** TGTACAAGACAACTCGGA-3'
T1-S3	5'-GAAGATTATCCAAAGAGA GCTTGATGTATCTTCAGG **T** CACAGATACTAGCCTACC-3'
T2-S1	5'-GAAGATTATCCAAAGAGA TCCGAGTTGTCTTGTACA **TT** CCTGAAGATACATCAAGC-3'
T2-S2	5'-GAAGATTATCCAAAGAGA GGTAGGCTAGTATCTGTG **TT** TGTACAAGACAACTCGGA-3'
T2-S3	5'-GAAGATTATCCAAAGAGA GCTTGATGTATCTTCAGG **TT** CACAGATACTAGCCTACC-3'
T3-S1	5'-GAAGATTATCCAAAGAGA TCCGAGTTGTCTTGTACA **TTT** CCTGAAGATACATCAAGC-3'
T3-S2	5'-GAAGATTATCCAAAGAGA GGTAGGCTAGTATCTGTG **TTT** TGTACAAGACAACTCGGA-3'
T3-S3	5'-GAAGATTATCCAAAGAGA GCTTGATGTATCTTCAGG **TTT** CACAGATACTAGCCTACC-3'

Table S3. Oligonucleotide sequences of the non-matching T1-triskelion ($T1_{no\text{-}match}$) used as a control in DLS and AGE.

Oligo name	Sequence
$T1_{no\text{-}match}$-S1	5'- GACTATTCTATTAATTTA TCCGAGTTGTCTTGTACA **T** CCTGAAGATACATCAAGC-3'
$T1_{no\text{-}match}$-S2	5'-GACTATTCTATTAATTTA GGTAGGCTAGTATCTGTG **T** TGTACAAGACAACTCGGA-3'
$T1_{no\text{-}match}$-S3	5'-GACTATTCTATTAATTTA GCTTGATGTATCTTCAGG **T** CACAGATACTAGCCTACC-3'

Table S4. Oligonucleotide sequences of the removable triskelion. The 5'-ends were labeled with an ATTO550N fluorophore each for the fluorescence-quenching experiments (as described in section S4).

Oligo name	Sequence
T1s-S1	5'-GTGTTCGGTCTATCCAAAGAGA TCCGAGTTGTCTTGTACA **T** CCTGAAGATACATCAAGC-3'
T1s-S2	5'-GTGTTCGGTCTATCCAAAGAGA GGTAGGCTAGTATCTGTG **T** TGTACAAGACAACTCGGA-3'
T1s-S3	5'-GTGTTCGGTCTATCCAAAGAGA GCTTGATGTATCTTCAGG **T** CACAGATACTAGCCTACC-3'

Table S5. Oligonucleotide sequence of the displacement strand S and the non-hybridizing control $S_{control}$. BHQ2 signifies the position of the Black Hole II quencher.

Oligo name	Sequence
S	5'- TCTCTTTGGATAGACCGAACAC-3'/BHQ2
$S_{control}$	5'- TGAATCTAACGGTGCGTATCTC-3'/BHQ2

The linker was folded at a concentration of 4 μM (equimolar) in 1x PBS (pH = 7.4). For optimized folding of the linker, the following thermal program was used:

1. Heating to 70 °C
2. Temperature ramp from 70 °C to 25 °C in 90 steps of -0.5 °C /30 sec each
3. Hold at 4 °C

The triskelion was folded at a concentration of 6 μM (equimolar) in 1x PBS (pH = 7.4) using the following thermal protocol:

1. Heating to 95 °C and hold for 2 min
2. Cooling to 85 °C and hold for 3 min
3. Cooling to 80 °C and ramping to 52 °C in 56 steps of -0.5 °C /30 sec each
4. Hold at 4 °C

S2. Characterization of the individual DNA structures (linker and triskelion)

a. *Polyacrylamide gel electrophoresis*

To evaluate the folding success the DNA structures, polyacrylamide gel electrophoresis (PAGE) was performed. For all studied structures predominantly single bands were found, indicating a high yield of the desired product (Figure S1). The gel was prepared with 10% polyacrylamide and run for 60 min at 100 V, immersed in a solution containing 11 mM $MgCl_2$ buffered at pH = 8.3 with 0.5x TBE.

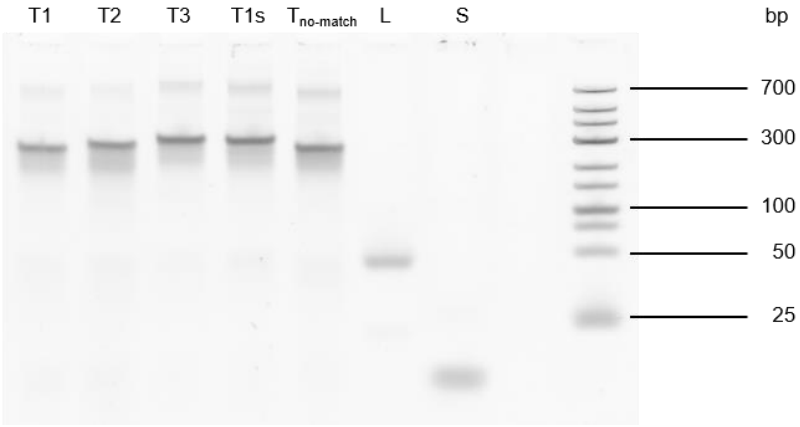

Figure S1. Polyacrylamide gel electrophoresis of the utilized DNA structures T1, T2, T3, T1s, $T_{no\text{-}match}$, L and S. T1, T2 and T3 refer to the three triskelion configurations. T1s refers to the removable triskelion. $T_{no\text{-}match}$ describes the non-matching triskelion used for controls. L stands for the linker and S for the displacement strand S. The structures were run alongside a GeneRuler Low MW (Thermo Fisher Scientific) DNA ladder.

b. Atomic force microscopy

The three configurations T1, T2, T3 of the triskelion were additionally investigated by atomic force microscopy (AFM) in solution (Figure S2, Figure S3a), showing the expected star-like shape with three arms extending from the center of the DNA structures. The T2 triskelion was also imaged in solution after incubation with the linker (L, Figure S3b). Through the incubation with L, the triskelion structures underwent elongation and oligomers were detected. Here, no large-scale networks were encountered presumably due to the substantially decreased concentrations employed for the incubation (100-fold dilution of both T2 and L).

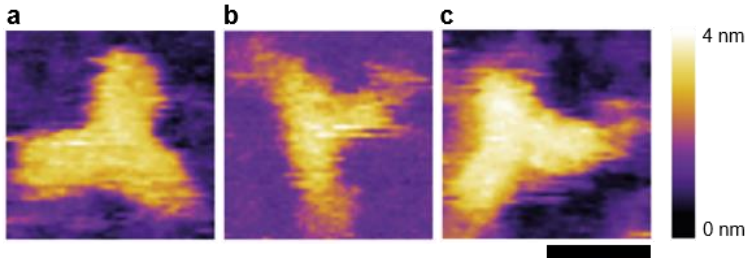

Figure S2. AFM topographical images of the triskelion designs acquired in solution. T1 (a), T2 (b), T3 (c). Scale bar: 10 nm.

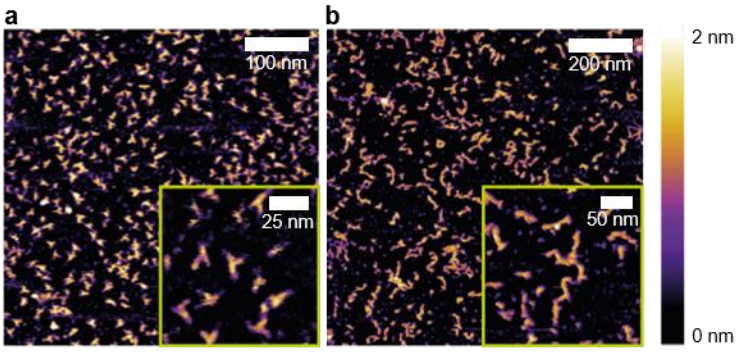

Figure S3. Topographical AFM images of the triskelion T2 (a) before and (b) after linker addition. In both (a) and (b) images, a higher magnification of the DNA structures is shown in the insets.

c. Agarose gel electrophoresis

To evidence the ability of the different triskelion designs to interconnect with L , agarose gel electrophoresis (AGE) was performed with incubations of the linker without the Chol-TEG tag (L-) and four triskelion configurations (T1, T2, T3, T1s; Figure S4). Hereby, 0.5% agarose gels were prepared in a solution containing 11 mM $MgCl_2$ buffered at pH = 8.3 with 0.5x TBE. The gel was run for 120 min at 60 V. For all four designs three incubation conditions were selected: the same molar ratio of L/T as present in the vesicle coating fabrication (LT,1x), half the triskelion concentration (LT,0.5x) or 1.5x the triskelion concentration (LT,1.5x, all incubations for 50 min at 4 °C). The incubations involving T1, T2, T3, and T1s show strong aggregation in the pockets and very limited penetration of the gel (Figure S4a). By contrast, incubating the linker with the $T_{no\text{-}match}$ triskelion under the same three conditions did not result in strong aggregation and clearer bands in the gel (Figure S4b). This indicates that the DNA aggregates due to the intended Watson-Crick hybridizations between the sticky ends of the linker and triskelion instead of unspecific stacking.

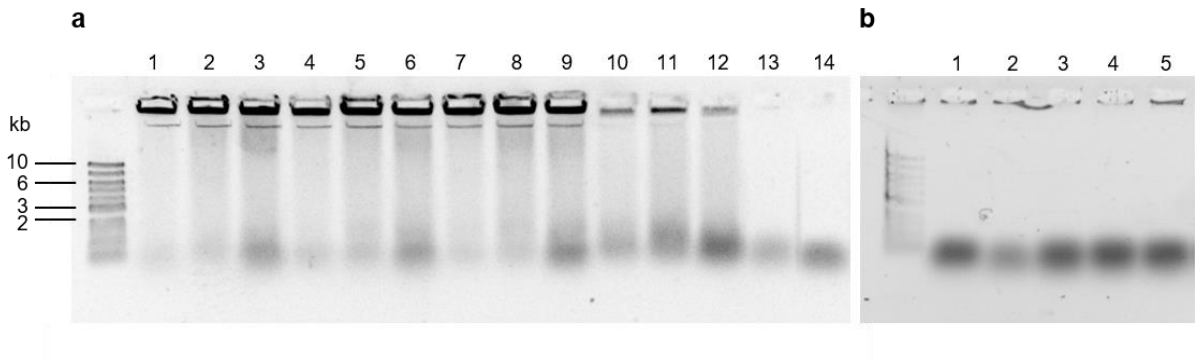

Figure S4. Agarose gel electrophoresis describing the linker-triskelion interaction. (a) 10 kbp ladder, the linker-triskelion incubations LT1,0.5x (1), LT1,1x (2), LT1,1.5x (3), LT2,0.5x (4), LT2,1x (5), LT2,1.5x (6), LT3,0.5x (7), LT3,1x (8), LT3,1.5x (9), LT1s,0.5x (10), LT1s,1x (11), and LT1s,1.5x (12) were run. As a comparison, the triskelion (13) and the linker (14) alone are shown. (b) The most left shows the same ladder as in (a). The lanes 1 to 5 include the $T_{no\text{-}match}$ triskelion (1) and the linker (2) next to the mixtures of the linker in varying ratios to the $T_{no\text{-}match}$ triskelion: $LT_{no\text{-}match}$,0.5x (3), $LT_{no\text{-}match}$,1x (4), $LT_{no\text{-}match}$,1.5x (5).

S3. Characterization of the DNA-liposome hybrid structures

a. Dynamic light scattering and zeta potential measurements

Figure S5 gathers the size distributions of V, VL, VLT1, VLT2, VLT3 corresponding to the averaged values shown in Figure 1e of the main text.

To demonstrate that the DNA assembly on the liposome surface was not produced by electrostatic interactions but required the presence of cholesterol anchors of the linkers and the appropriate complementarity of the sticky ends, three controls were investigated.

The first control was prepared by incubating V with the linker omitting the cholesterol-TEG modification and further addition of T1. The resulting structure, VL-T showed a similar hydrodynamic diameter in dynamic light scattering (DLS; with 183 ± 8 nm, Figure S6) and ζ-potential (with -5 ± 1 mV) to plain liposomes (V: 195 ± 10 nm and -4 ± 1 mV).

The second control was achieved by incubating VL (linker with cholesterol-TEG modification) with a triskelion with sticky ends of a different sequence to not hybridize with the linker ($T_{no\text{-}match}$, sequences gathered in Table S3). Indeed, $VLT_{no\text{-}match}$ exhibited a similar average size (Figure S6, 188 ± 5 nm) and ζ-potential (-20 ± 2 mV) to VL (190 ± 10 nm, -19 ± 2 mV).

Finally, to assess any aggregation or apparent liposome coating induced by unspecific adsorption of the triskelion to the bilayer, DLS of vesicles with increasing concentrations of the T1 triskelion (VT, with no linker involved) was measured. No size increase could be detected up to 4.3 μM which corresponds to a seven-fold of the concentration used in the formation of VLT (620 nM) (Figure S7)

The incubation of the linker with the triskelion in absence of vesicles (LT1) lead to a broad distribution of sizes without a defined peak (Figure S6), underpinning the templating function of the vesicles. Averaged diameters and ζ-potential are all gathered in Table S6.

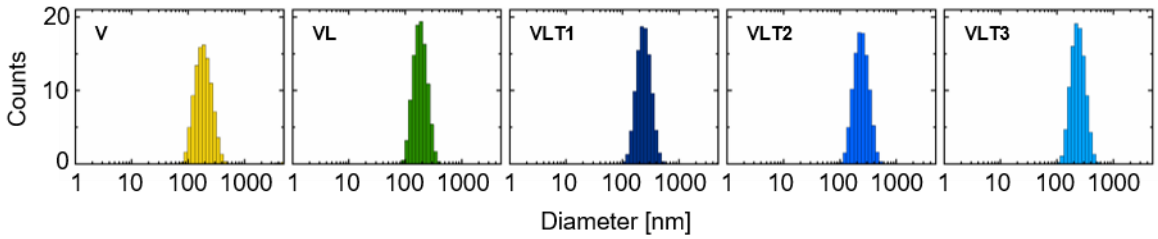

Figure S5. Hydrodynamic diameters measured by DLS of (a) V, (b) VL, (c) VLT1, (d) VLT2, and (e) VLT3. Counts shown in intensity.

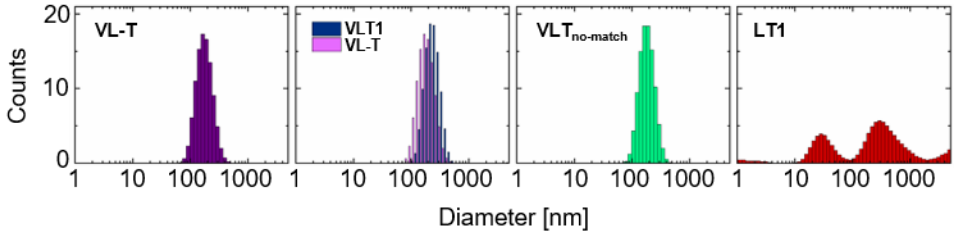

Figure S6. Hydrodynamic diameters measured by DLS of VL-T, $VLT_{no\text{-}match}$, linker and the T1 triskelion incubated without the vesicles (LT1), as indicated. As a reference, an overlay of VL-T and VLT1 is shown. Counts shown in intensity.

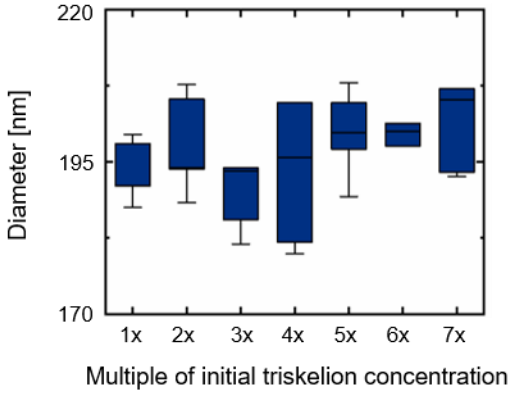

Figure S7. DLS of vesicles and the T1 triskelion to assess size changes induced by adsorption of the DNA structure with no linker. The boxplot of the sizes measured at multiples of the original triskelion concentration (620 nM, as used in the study) does not show any correlated size increase (black lines indicating the median).

Table S6: Average sizes (diameter in nm) measured by DLS and zeta potential (in mV) of V, VL, the hybrid structures, and controls.

Sample	V	VL	VLT1	VLT2	VLT3	VLT1s	VL-T	$VLT_{no\text{-}match}$
size	195 ± 10	190 ± 10	247 ± 6	248 ± 8	245 ± 7	246 ± 13	183 ± 8	188 ± 5
ζ-potential	-4 ± 1	-19 ± 2	-31 ± 2	-31 ± 2	-32 ± 2	-31 ± 2	-5 ± 1	-20 ± 2

b. Cryo-electron microscopy

Figure S8 shows additional cryo-EM micrographs. The incubation of the vesicles and the linker (VL, Figure S8) leads to the accumulated appearance of structures describable as short spikes or black dots at the surface of the liposomes. The top row of Figure S8 displays the DNA triskelion interconnected with L (after incubating for 50 min at 4 °C and in absence of the LUVs), rendering a mesh of the DNA components over large areas of the grid. The completed hybrid structures VLT1, VLT2 and VLT3 show a clear DNA corona (Figure S8) which is not observed in the case of VL (or V).

Figure S9 shows the VLT1s structures before (a ,b, c) and after (d, e) addition of the displacement strand.

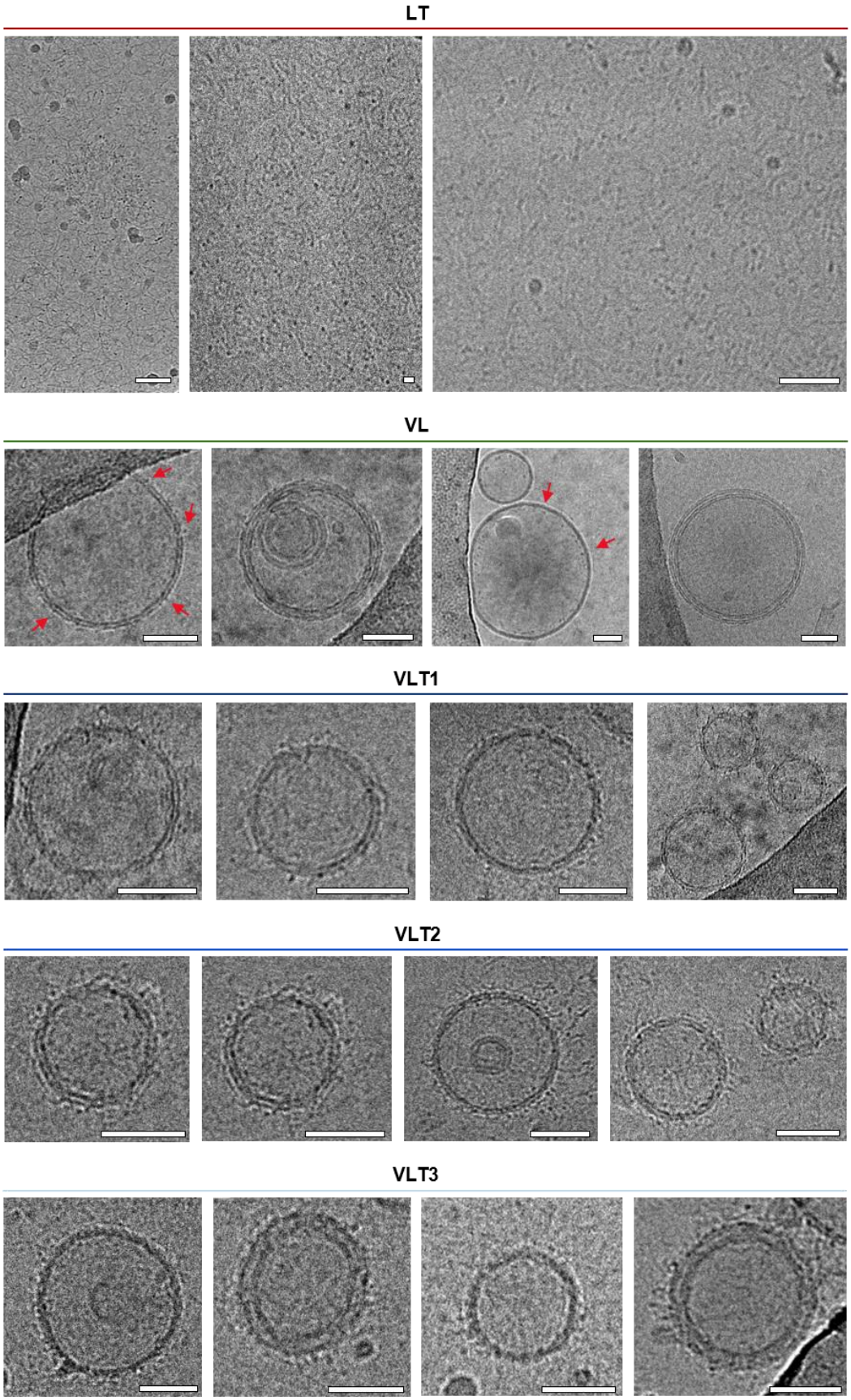

Figure S8. Further cryo-EM micrographs visualizing LT, VL, VLT1, VLT2, and VLT3. Scale bars: 50 nm.

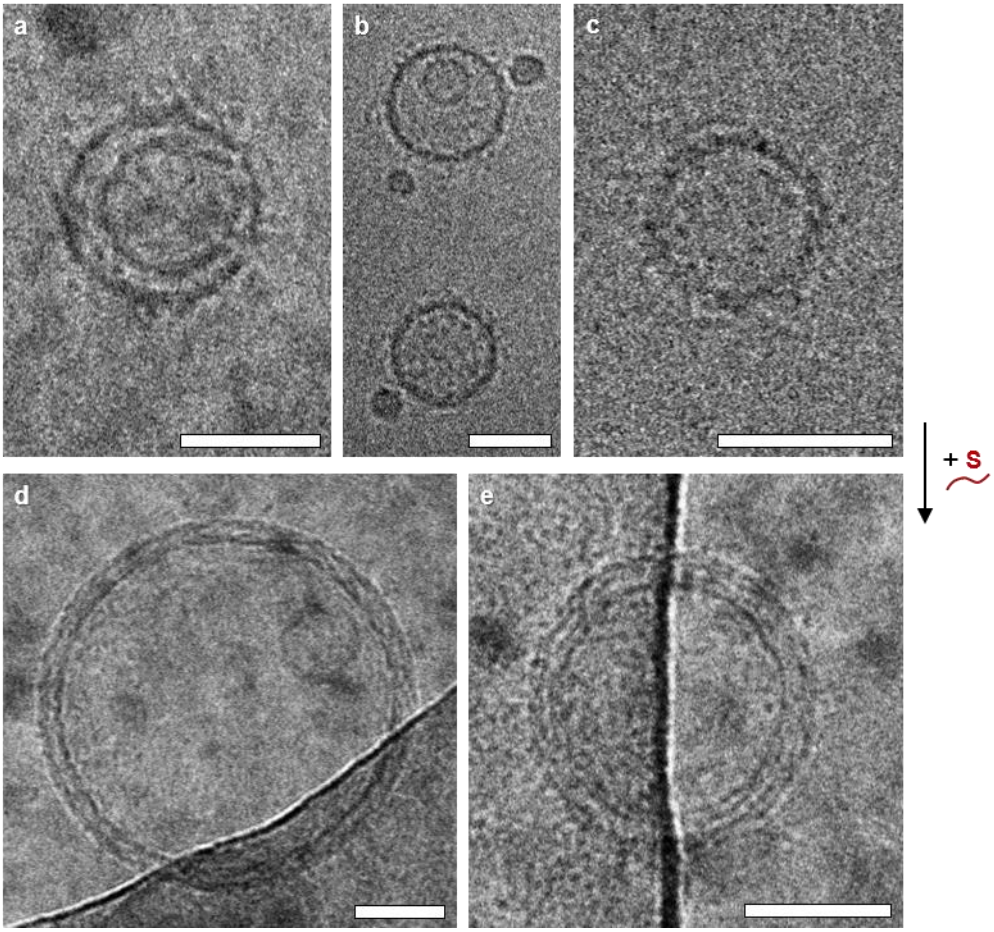

Figure S9. Cryo-EM micrographs illustrating the toehold-mediated coating disassembly. VLT1s (a to c), VLT1s + S (d and e). Scale bars: 50 nm.

c. *Atomic force microscopy*

Figure S10 shows representative AFM micrographs of the VLT2 and VLT3 designs.

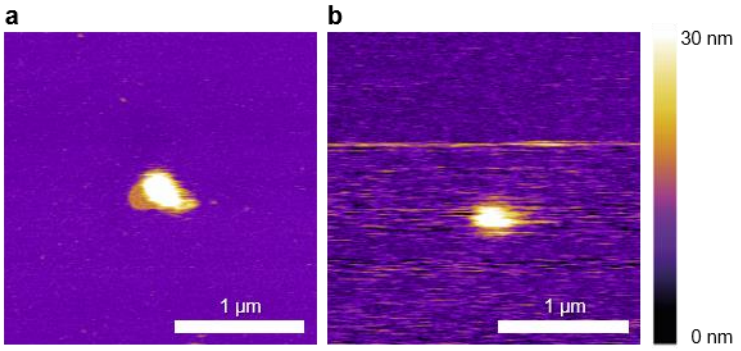

Figure S10. Micrographs of VLT2 (a) and VLT3 (b) on mica, subjected to the incubation protocol described in the experimental section of the main text.

To provide further evidence of the mechanically protective properties of the DNA coating, an alternative sample incubation protocol was used: the samples were incubated under the same buffer and salt conditions (5 mM $MgCl_2$ and 3 mM Tris-HCl, pH = 7.4, for details see experimental section) however at 30 °C for 30 minutes and cooled down to 25 °C for another 30 min.

Regardless of the incubation protocol chosen (alternative versus protocol reported in experimental section), V formed a bilayer covering the substrate. VL showed the same behavior except for spreading comparably more slowly, which resulted in partial coverage of the grid after the incubation time. Spherical structures were only detected for VLT and in both protocols, independently of the triskelion configuration involved. Figure S11 shows representative results for V, VL and VLT subjected to the incubation protocol starting at 30 °C and cooling to 25 °C for 30 min. No clear differences in the outcome compared to the other protocol, as presented in the main text (Figure 4), could be observed.

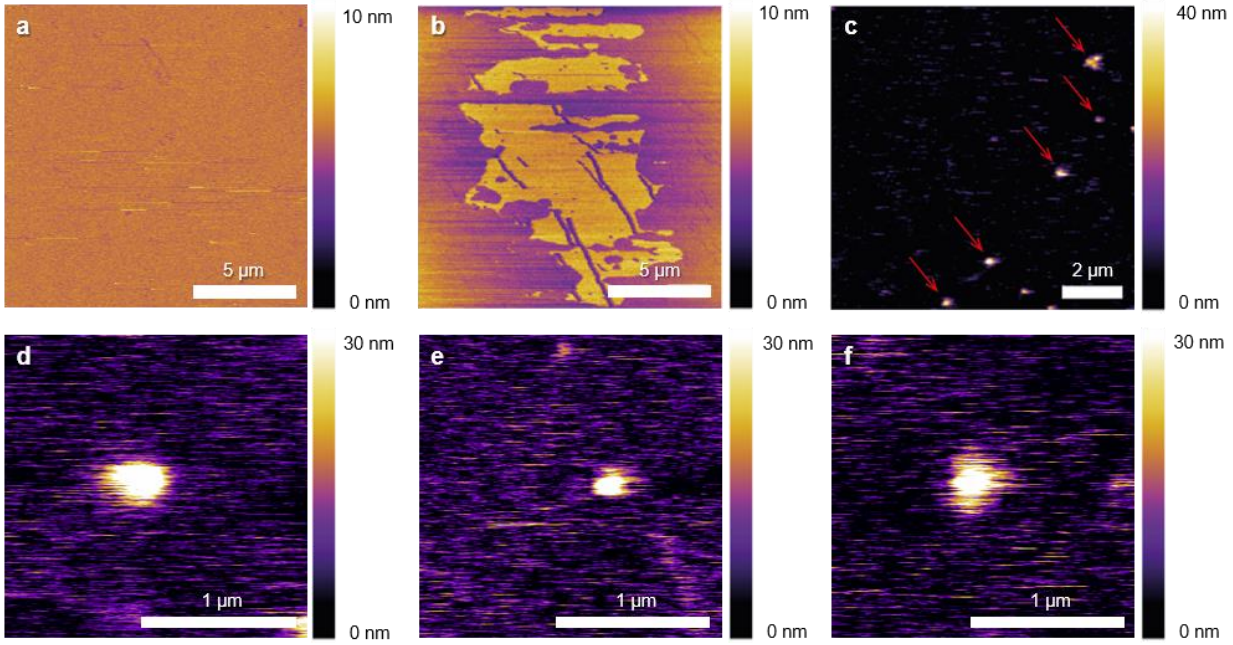

Figure S11. Samples in AFM subjected to the alternative incubation protocol. (a) V covers the whole substrate with a lipid bilayer. (b) VL forms bilayers partially covering the mica surface, with occasional long stripes produced by the AFM tip dragging vesicles across the surface during imaging. Only the hybrid structures remain stable (b), here shown for VLT1 (red arrows). Higher magnifications show single DNA-coated vesicles can be obtained for VLT1 (d), VLT2 (e), and VLT3 (f).

The mechanical properties of the hybrid structures were quantified by force spectroscopy with the AFM tip used as a nano-indenter. Force-distance curves (FD curves) were acquired with the tip located directly atop the vesicles to measure the force applied as a function of the tip vertical displacement. FD curves were conducted for the three different configurations (VLT1, VLT2, VLT3) and complemented in each case by AFM imaging to ensure validity of the results and correct positioning of the tip on the vesicles. Reliable FD curves could be easily distinguished from ambiguous measurements by considering the noise of baseline and the clarity of the rupture

event (Figure S12). The experiments were repeated 3 times for each sample with at least 10 reliable FD curves per sample. Figure S12 gives a representative example of reliable (a) and discarded (b) FD curves. The reliable FD curve exhibits a clear rupture event and coincident baselines in extension and retraction. The rupture event is not clear in Figure S12b where the extension/retraction baselines do not coincide, likely due to the tip compressing the side of a vesicle or a partially broken structure. In reliable measurements, the rupture event appears as a single or double event, depending on whether the AFM tip ruptures only one or both the top and the bottom layer of the compressed vesicle. The analysis was conducted by fitting with a mathematical model[1] the region of the curve where the tip compresses the structure, but no rupture event has taken place yet (Figure S12). This ensures that the Young's modulus is calculated only for intact vesicles. The rupture force can be obtained from the first rupture event, but we found it to be a poor predictor of the overall vesicles stability due to a high vulnerability to the precise compression geometry (tip shape, tip localization on the vesicle, etc.). Therefore, only the Young's modulus was determined as a more reliable indicator of the vesicles stability, corresponding to their reversible elastic deformation. The Young's modulus values derived for each curve were averaged and the uncertainty taken as the standard error on the means.

In addition to VLT1, VLT2, and VLT3, Figure S13 includes the Young's modulus of VLT1s. Showing a value of 2.1 ± 0.2 kPa, VLT1s represents the softest structure compared to the other coatings.

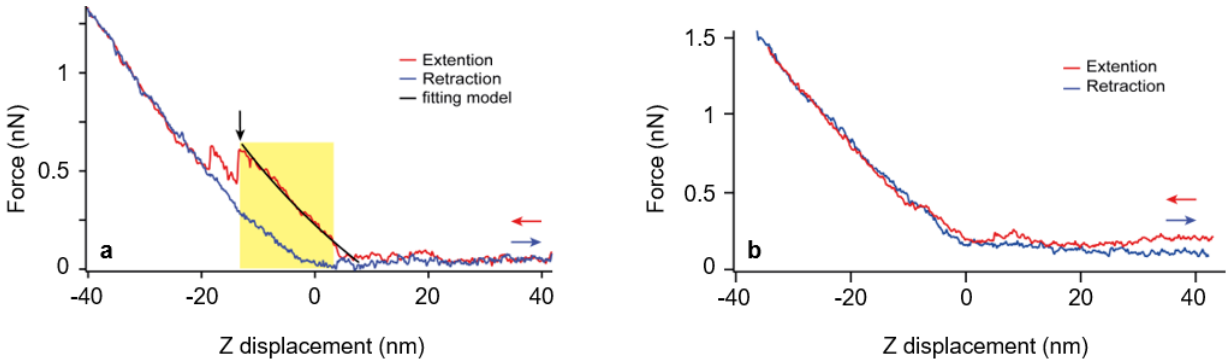

Figure S12. Example of FD curves used for calculating the Young's modulus. (a) The abrupt rupture of the vesicle (black arrow) is clearly visible in the approach (red curve). This curve represents a reliable measurement and allows the calculation of the Young's modulus by using the indentation region prior to the vesicle rupture (highlighted). (b) Example of an ambiguous FD-curve discarded due to the absence of a visible rupture event.

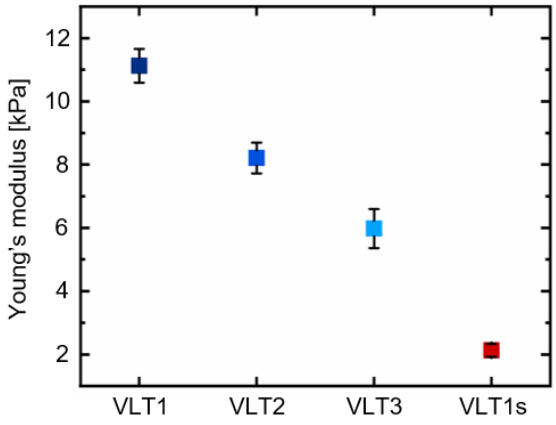

Figure S13. Young's moduli of the hybrid structures including the responsive VLT1s design.

S4. Confocal microscopy and fluorescence recovery after photobleaching on GUVs

Fluorescence recovery after photobleaching (FRAP) measurements were performed on DNA coated giant unilamellar vesicles (GUVs). These measurements were conducted using a Leica TCS SP5 II confocal microscope (Leica) and a 100X oil immersion objective.

To exclude the possibility of signal generation due to Mg^{2+}-mediated non-specific adsorption of the triskelion instead of intended cholesterol-facilitated interactions, the triskelion was labeled with 3 ATTO647N dyes per structure and incubated with the GUVs. Figure S14 (VT1, bottom row) shows that only weak adsorption could be detected, as the signal is not significantly above the detection limit.

In order to confirm large-scale interconnection of the triskelion with the linker, we investigated the mobility of the DNA network on the GUVs by FRAP measurements on VL, VLT1, VLT2, VLT3 and $VLT_{no\text{-}match}$ (the completely non-hybridizing triskelion). Hereby, one of the two strands comprising the linker was labeled with an ATTO647N fluorophore. A 3 μm diameter circular area was bleached into the DNA coat at the bottom of the GUVs. The recovery rates of the linker (VL) or the entirely non-hybridizing triskelion ($VLT_{no\text{-}match}$) were too high to be measured with the given setup and signal conditions (data not shown). Figure S15 shows representative images of VLT1, VLT2, and VLT3 before and after bleaching.

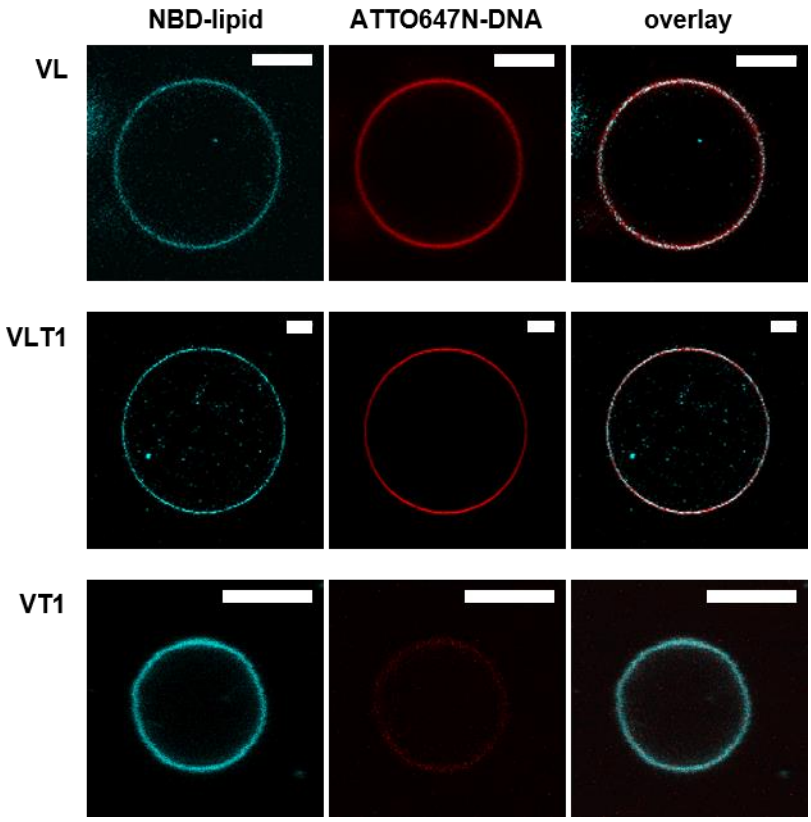

Figure S14. Cross-sectional confocal micrographs of the GUVs with the linker only (top row), the coat involving the T1 design (middle row), and only the T1 triskelion to assess Mg^{2+}-mediated adsorption. VL and VLT1 show that the DNA is colocalized with the GUVs, evidencing the cholesterol-facilitated attachment. T1 only adsorbs weakly, as the DNA fluorescence colocalized with the GUVs is only insignificantly higher than the background. Scale bars: 5 μm.

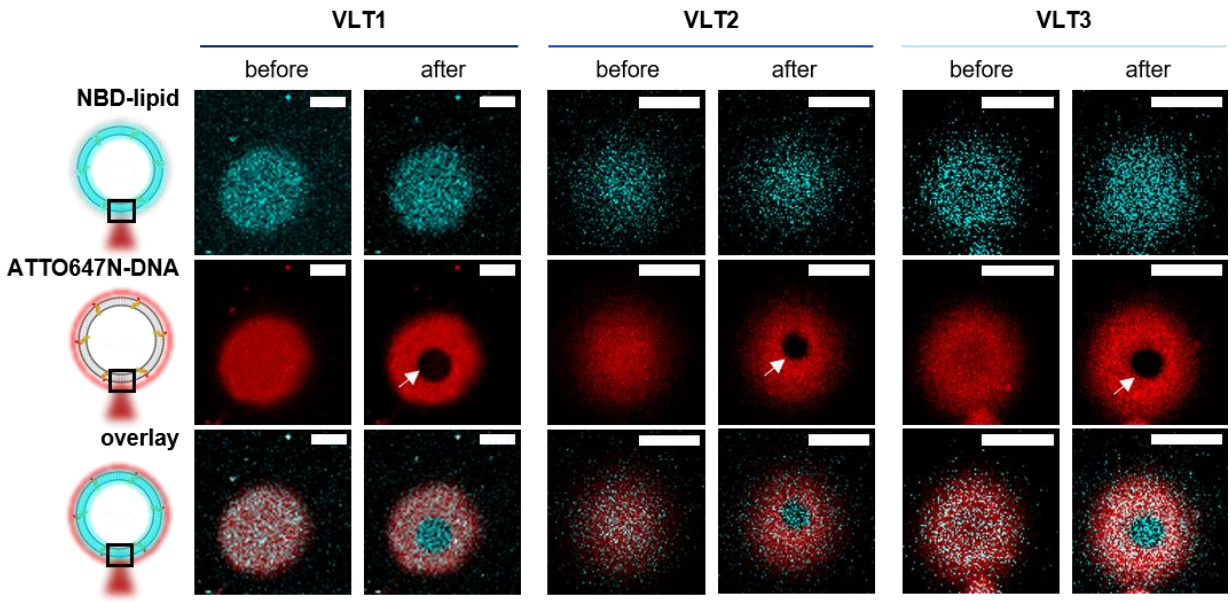

Figure S15. Confocal micrographs comparing the DNA-coated vesicles before and after bleaching the ATTO labels of the linkers. Since a 635 nm laser was irradiated, the NBD-labeled lipids do not show significant bleaching. The ATTO-labeled linker integrated in the finalized DNA coat does not recover after bleaching as indicated by the arrows, where a circular area of the bleaching spot can be seen. Scale bars: 5 μm.

FRAP experiments on two extra coating conditions in which one or two unmatching arms (no complementarity with the linker), as presented in Figure 3 (main text), restricting the formation of an extended network, were involved modifying the T1 triskelion as shown below (Figure S16, sequences can be reviewed in Table S7 (strands T1-1 and T1-2).

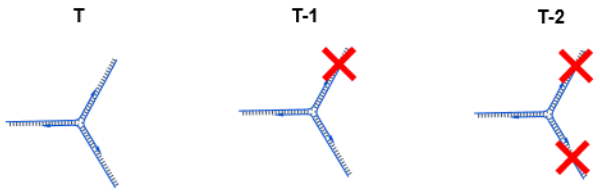

Figure S16. Triskelion modifications with intentionally limited hybridization abilities. To restrict interactions with the linkers, the sequences of one or two, arms were changed to avoid hybridization with the linker.

Table S7. Oligonucleotide sequences of the modified triskelion arms.

Oligo name	Sequence
T1-1	5'- GACTATTCTATTAATTTA TCCGAGTTGTCTTGTACA **T** CCTGAAGATACATCAAGC-3'
T1-2	5'-GACTATTCTATTAATTTA GGTAGGCTAGTATCTGTG **T** TGTACAAGACAACTCGGA-3'
T2-1	5'- GACTATTCTATTAATTTA TCCGAGTTGTCTTGTACA **TT** CCTGAAGATACATCAAGC-3'
T2-2	5'- GACTATTCTATTAATTTA GGTAGGCTAGTATCTGTG **TT** TGTACAAGACAACTCGGA-3'
T3-1	5'- GACTATTCTATTAATTTA TCCGAGTTGTCTTGTACA **TTT** CCTGAAGATACATCAAGC-3'
T3-2	5'- GACTATTCTATTAATTTA GGTAGGCTAGTATCTGTG **TTT** TGTACAAGACAACTCGGA-3'

S5. Triggered disassembly of the DNA coat by toehold displacement of the triskelion

a. Polyacrylamide gel electrophoresis

The functionalization of the network, achieved by toeholds added to the triskelion arms (new design referred to as T1s), was examined with respect to the effect of the displacement strand S in different concentrations by PAGE. Figure S17 gathers lanes showing the involved structures individually and the effects of S addition on the LT1s network. Lanes 1 to 3 show the bands provided by S, L and T1s. The addition of S to T1s renders a band with a retarded migration (lane 4), indicating the attachment of the displacement strand to the triskelion. The linker and the displacement strand do not interact, as lane 5 reveals. In the absence of V, the mixture of L and T1s incubated under the same conditions as for the VLT1s, leads to strong aggregation of the structure and restricted penetration of the gel (lane 6). In lanes 7 a to c, S was added to the LT1s mixture in a 1:1 (a), 2:1 (b), and 3:1 ratio (c). Lane 8 includes the linker for direct comparison to the samples in lanes 7a to c where S was added. As visible in lanes 7a to c, the addition of S causes the disaggregation of LT1s, proving the success of the toehold displacement. Already the 1:1 ratio prove to be sufficient for full disassembly.

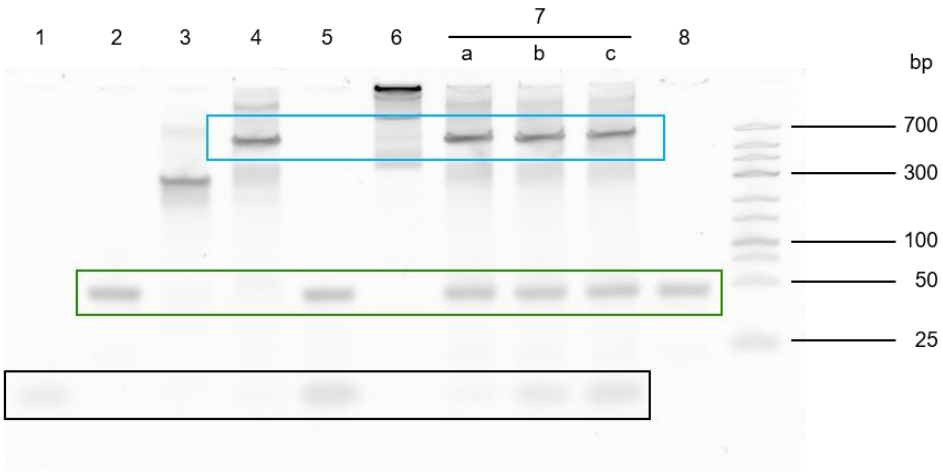

Figure S17. Gel electrophoresis probing the triskelion displacement. The lanes show: S (1); L (2); T1s (3); S+T1s (4); L+S (5); L+T1s (6); LT1s+S in a 1:1 (7a), 2:1 (7b) and 3:1 (7c) molar ratio in; L (8). Bands corresponding to either T1s+S, L or S are marked with a blue, green and black rectangle respectively.

S6. Effect of detergent addition on the hybrid structures

a. Electron microscopy

In order to determine the nature of the particles detected by DLS after TX100 addition (main text, Figure 6), we imaged V and VLT1 samples through cryo-EM and negative staining TEM. Experimental details concerning the former can be found in the experimental section of the main text. Negative staining samples were prepared by incubating 10µL of sample at 0.8mg/ml for 1 minute on a Cu 400 mesh grid covered with a layer of amorphous carbon. The sample was then stained with a 1% uranyl acetate solution and imaged with a FEI Tecnai T20 microscope operated at 200kV at a magnification yielding 8 Å/pixel at specimen level (using a Veleta detector). While solubilization of V is observed upon 0.5% TX100 addition (Figure S18, Figure S19), the addition of TX100 to VLT1 results in larger particles (Figure S20). Since the morphology of these particles substantially differs from the original VLT1, we assign them as DNA-assemblies that remain at least partially interconnected.

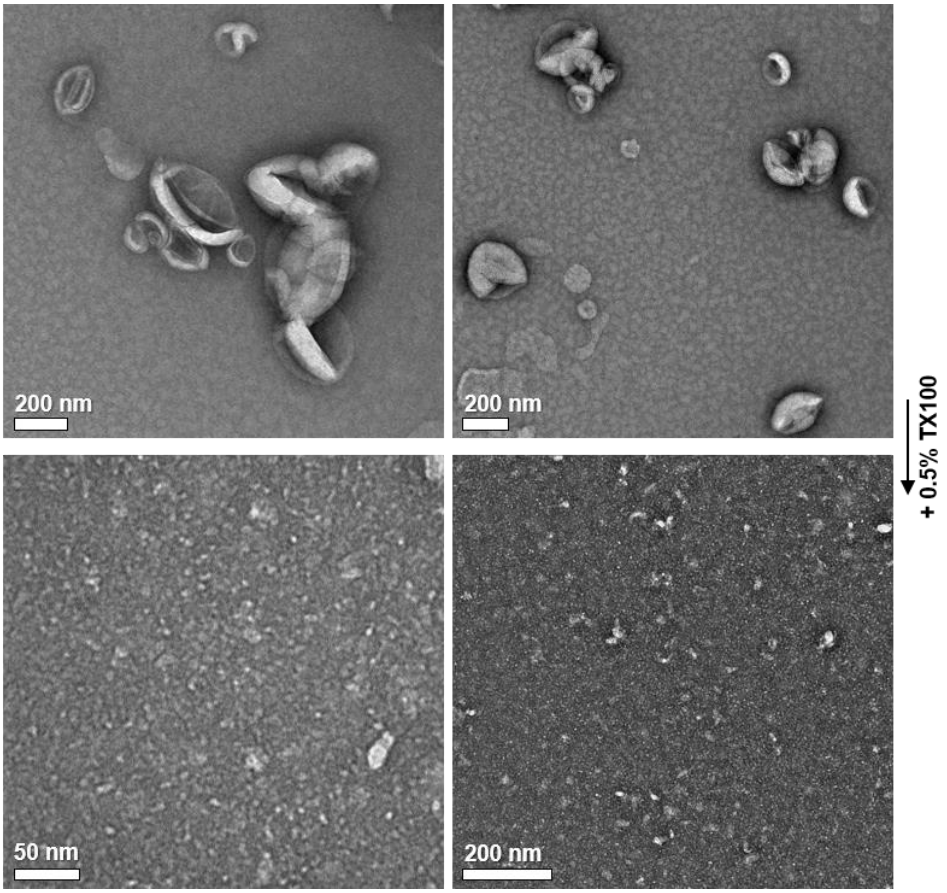

Figure S18. Negative-staining electron micrographs of V before (top) and after (bottom) TX100 addition.

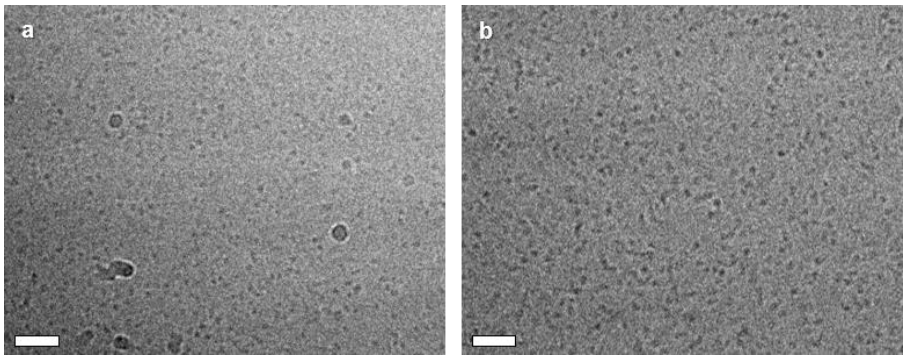

Figure S19. Cryo-EM micrographs of V (a) and VL (b) after X100 addition. Scale bars: 50 nm.

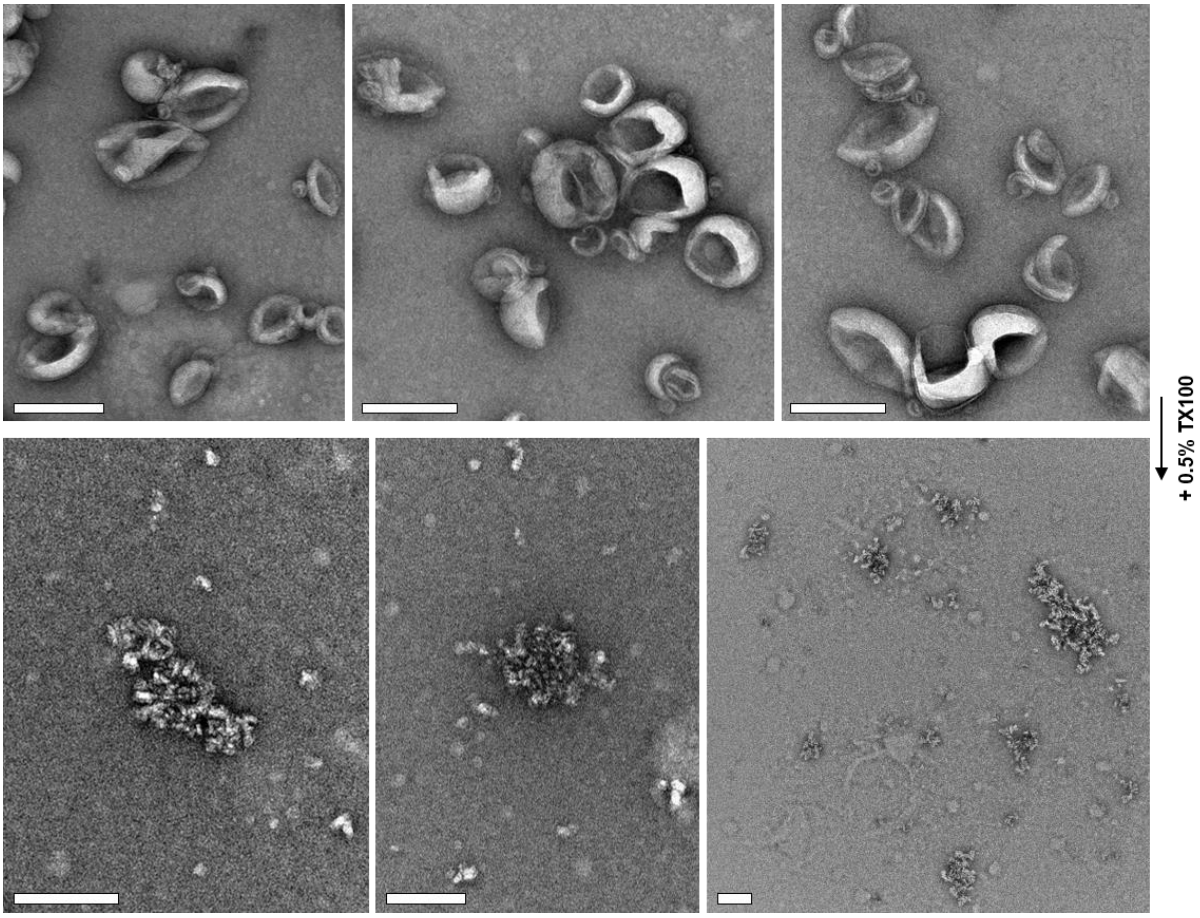

Figure S20. Negative-staining electron micrographs of VLT1 before (top) and after (bottom) TX100 addition. Scale bars: 200 nm.

b. Dynamic light scattering

The addition of 0.5% TX100 to V and VL led to a single peak centered at 12 nm (Figure 4a and b, main text) considered to originate from micelle-like (triton and triton-lipid complexes) structures. According to supplier data (Sigma Aldrich) and previous studies[4], the employed TX100 concentration was above the critical micelle concentration (cmc). Indeed, an equal hydrodynamic diameter of approximately 12 ± 1 nm was measured for 0.5% TX100 purely diluted in PBS (Figure S20). The same behavior is observed upon addition of 0.5% TX100 to the $VLT_{no\text{-}match}$ sample (Figure S21). On the contrary, the addition of 0.5% TX100 to either VLT1 (Figure 5c in the main

text), VLT2, or VLT3 (Figure S21) shows a peak that has been assigned to the presence of DNA assemblies partially interconnected.

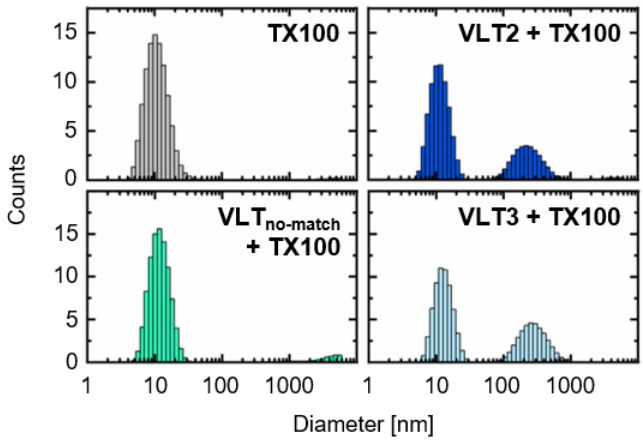

Figure S21. Hydrodynamic diameters of TX100-treated samples measured by DLS of 0.5% Triton X-100 in PBS, 0.5% TX100 added to $VLT_{no\text{-}match}$, VLT2 with 0.5% TX100, and VLT3 with 0.5% TX100, as indicated. Counts in intensity.

Linker and triskelion concentrations used for the coating were set to 930 nM and 620 nM, respectively (ratio 3:2 for linker/triskelion). We investigated how the use of different linker and triskelion concentrations for the coating could affect the response of VLT to TX100. On the one hand, the linker concentration was kept constant (930 nM) while the triskelion concentration was varied to render 310 nM and 930 nM. On the other hand, the triskelion concentration was fixed (620 nM) whereas the linker concentration was adjusted to 232.5 nM, and 1395 nM. For both experiments the size distribution was tracked in DLS before and after the addition of TX100. Figures S22 and S23 gather these data. When the concentration of either linker or triskelion is lower than the one required to obtain a ratio (3:2, linker/triskelion) no significant peak assigned to remaining DNA assemblies is observed after TX100 addition.

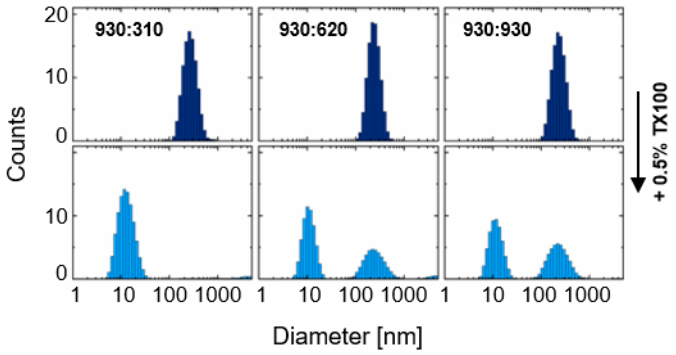

Figure S22. DLS data for LUVs coated with different triskelion concentrations (top panel, dark blue graphs) and the effect after the addition of triton (bottom panel, light blue graphs).

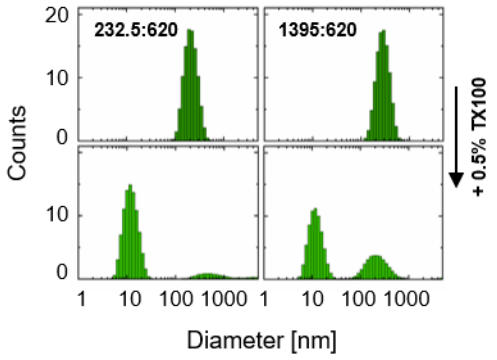

Figure S23. DLS data for LUVs coated with different concentrations of linker (top panel, dark green graphs) and the effect after the addition of triton (bottom panel, light green graphs).

The behavior upon addition of TX100 was also applied for liposomes coated with triskelion structures designed to restrict the interactions with the linker by modifying the sequence of either 1 or 2 arms of the triskelion (Figure S16). This led to the structures VLTx-1 and VLTx-2 (with x=1, 2, 3 referring to T1, T2 and T3 and -1, -2 denoting either 1 or 2 modified arms; the sequences can be reviewed in Table S7). For each version, the size distribution was measured by DLS before

and after TX100 addition. The results are gathered in Figure S24. As opposed to the original hybrid structures VLT1, VLT2, VLT3, none of the modified structures could render larger particles upon TX100 addition (assigned to the presence of remaining DNA assemblies). These findings support the importance of maximizing the interactions between linker and triskelion to favor LUV coating.

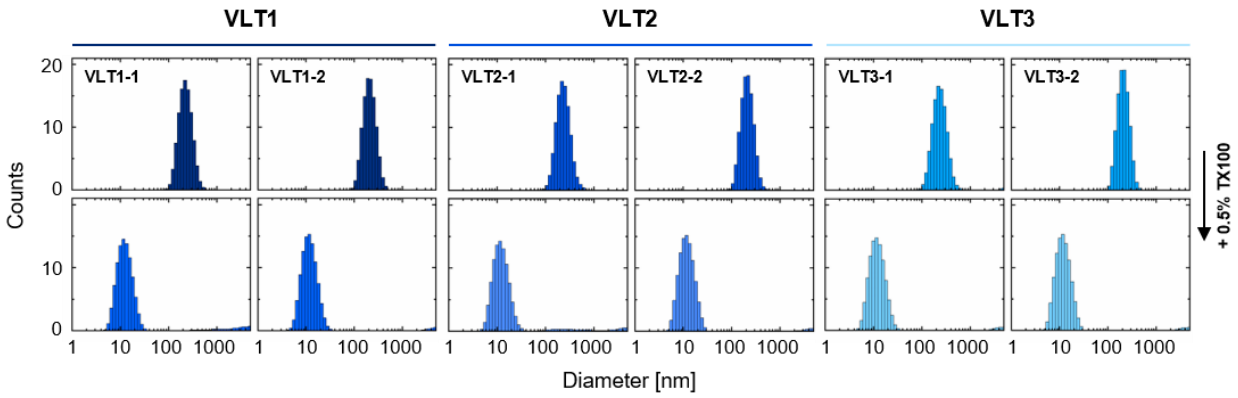

Figure S24. Triton addition to the incompletely assembled hybrid structures depending on the involved triskelion design.

Supporting references

(1) Laney, D. E.; Garcia, R. A.; Parsons, S. M.; Hansma, H. G. Changes in the Elastic Properties of Cholinergic Synaptic Vesicles as Measured by Atomic Force Microscopy. *Biophys. J.* **1997**, *72*, 806–813.

(2) Castro, C. E.; Kilchherr, F.; Kim, D.-N.; Shiao, E. L.; Wauer, T.; Wortmann, P.; Bathe, M.; Dietz, H. A Primer to Scaffolded DNA Origami. *Nat. Methods* **2011**, *8*, 221.

(3) Kučerka, N.; Tristram-Nagle, S.; Nagle, J. F. Structure of Fully Hydrated Fluid Phase Lipid Bilayers with Monounsaturated Chains. *J. Membr. Biol.* **2006**, *208*, 193–202.

(4) Tiller, G. E.; Mueller, T. J.; Dockter, M. E.; Struve, W. G. Hydrogenation of Triton X-l 00 Eliminates Its Fluorescence and Ultraviolet Light Absorption While Preserving Its Detergent Properties. *Anal. Biochem.* **1984**, *266*, 262–266.